Supporting Information

# Additive Manufacturing of Complex Micro-architected Graphene Aerogels

*Ryan Hensleigh, Huachen Cui, James Oakdale, Jianchao Ye, Patrick Campbell, Eric Duoss, Christopher Spadaccini, Xiaoyu Zheng,* Marcus Worsley**

*Materials*: All materials were used as received. Graphene oxide (GO) was purchased from CheapTubes (single layer 1-20 um). Dimethylformamide (DMF, 99.8%), Bisphenol A ethoxylate (2 EO/phenol) dimethacrylate (BisA-EDMA) with an average molar mass of $M_n$ ~484, polyethylene glycol diacrylate $M_n$ ~700 (PEGDA700), ammonium hydroxide (28 - 30% in water), and phenylbis(2,4,6-trimethylbenzoyl)phosphine oxide (Irg819) were purchased from Sigma-Aldrich.

*Preparation of Photocurable Graphene Aerogel Resin*: In a typical preparation, 0.2 g GO was dispersed by ultrasonication in deionized water (20 g). GO crosslinking was catalyzed by 3.6 g of ammonium hydroxide (0.18 g/1 g GO dispersion) while heating at 80 °C for 96 h following previous reports. [19] After the reaction, the XGO hydrogel was washed by gently decanting and adding fresh deionized water, at least 3X for 12 h each. The XGO hydrogel was then exchanged with acetone, twice for 12 h, and finally with DMF twice for 12 h. Approximately 20 mL of solvent was used for each exchange, except the final DMF exchange which was set at 20 g for the final concentration (1 wt% or 10 mg/g of GO/DMF). The XGO hydrogel in DMF was broken up with a spatula to 1 to 5 mm diameter pieces, and then ultrasonicated for 24 h. To the XGO dispersion 1.2 g PEGDA700, 1.2 g BisA-EDMA, and 0.8 g Irg819 were added to make the XGO resin.

*Three-Dimensional Printing of Graphene Aerogel*: To print structures, we used a custom built system equipped with a 405 nm light source. A three-dimensional CAD model is sliced vertically into a series of layers. Using a spatial light modulator (SLM) as a dynamically reconfigurable digital photomask, each two-dimensional image slice is sequentially transmitted to the SLM which takes on the pattern of the image. Near-UV light illuminates the SLM from a photodiode, and a patterned beam is reflected. The patterned beam is reflected by a galvanometer mirror pair onto the photoresin. Where the two-dimensional image hits the resin, the material crosslinks and solidifies. Subsequently, the substrate on which the layer rests is lowered, thus reflowing a thin film of liquid over the cured layer. The image projection is then repeated, with the next image slice forming the subsequent layer. Parts of differing relative densities were made by varying the light exposure time of the parts, effectively producing parts with varying strut thicknesses.

*Bulk Sample Preparation*: Bulk samples for porosimetry were prepared by sandwiching the photocurable resin between glass slides with a small, ~0.5 mm spacer and curing in a broad spectrum light box (ELC-500) for 4 min on each side.

*Drying and Carbonization*: After printing, the resulting green gels were washed in DMF with sonication for a few min. They were then soaked in acetone for 24 h to remove all the DMF, exchanging the acetone several times. The wet gels were subsequently dried with supercritical $CO_2$ (Electron Microscope Sciences, EMS3100) for 24 h. For freeze-drying, green gels were washed in DMF with sonication for a few min. They were then rinsed with ethanol several times (a few mL for ~1 min) to remove DMF, and then soaked in water for 24 h, before freezing at -20°C. These frozen samples were lyophilized on a VWR lyophilizer for 24 h.

Samples were pyrolyzed at 1050°C under a $N_2$ atmosphere for 3 h, ramping up and down from room temperature at 1°C per minute. The graphene aerogel materials were isolated as black 3D carbon structures.

*Characterization*: Surface area was analyzed by Brunauer-Emmett-Teller nitrogen porosimetry using ASAP 2000 Surface Area Analyzer (Micrometrics Instrument Corporation). Samples from 0.05 to 0.1 grams were put under vacuum ($10^{-5}$ Torr) and heated at 150 °C for 24 h to remove adsorbed species before testing. Micro-Raman was done using a Renishaw inVia spectrometer with a 50x Leica objective and a 514 nm 9 mW $Ar^+$ laser. SEM samples were coated with Gold-Platinum alloy for 60s before imaging. TEM samples were prepared by crushing samples between glass slides, and poured onto a lacey carbon grid.

*Mechanical Testing*: Samples were tested in an Instron 5944 using standard flat compression plates (T1223-1022) and 500N load cell. Each sample was run through 5 cycles, at 2% strain each cycle, with a strain rate of 0.01% strain/min. Samples were tested on the [010] face, i.e. perpendicular to the build direction, to avoid support material which could lower the modulus. Data was extracted over less than 10% of the total loading or unloading curve, typically from the second or third cycle, to assure the Instron plate was fully attached to the sample. If the Z direction of a Cartesian coordinate system is the build direction, then the average X and Z of the lattice were determined by optical microscopy and used as the cross-sectional area, while the Y of the lattice was used as the length of the sample to calculate percent strain.

*Conductivity:* First, a MAG octet was surrounded by a square shaped strip of aluminum, leaving open two faces. Gold-Platinum alloy was sputtered on each opposite face of the lattice for 120s to produce an 8nm layer. The aluminum strip was removed, and the resistance from these faces was measured by a multimeter with simple needle test leads. The straight-line distance between each octet face, i.e. the width of the structure, was measured by optical microscopy, and use to convert resistance to conductivity.

*Scaling:* The relative density was measured by optical microscopy and previously derived formulas for stretch-dominated octet truss lattices.[1,2] These relative densities are only approximations, and for octet-truss the accuracy of the approximation depends on the relative density (RD). For lattice with RD less than 20%, the following formula was used where r is the radius of the strut, and l is the node-to-node length of the strut. A node is the intersection of struts.

$$RD = 6\sqrt{2}\pi\frac{r^2}{l^2}\left(1-\frac{8r}{9l}\right)$$

If the RD was greater than 20% using this formula, the following formula was used.

$$RD = 6\sqrt{2}\pi\frac{r^2}{l^2} - (\frac{16}{3})\sqrt{2}\pi\frac{r^3}{l^3}$$

Multiple measurements of the diameter and length were taken for each structure by optical microscopy before mechanical testing. The radius of the strut was calculated as half the diameter. The standard deviation of these measurements were used to calculate the error in relative density.

The RD fundamentally is density of the structure divided by density of equivalent solid

$$RD = \frac{\rho}{\rho_s}$$

To calculate absolute density, the density of a solid was multiplied by the calculated RD of the lattice. The solid was a 3D printed cube of the XGO resin, whose volume was calculated from its dimensions using optical microscopy, and mass was determined using multiple averaged measurements of a VWR electronic balance. The absolute density of a set of lattices were also tested by XP24, Mettler Toledo ultra-microbalance, and the results were within error for our method.

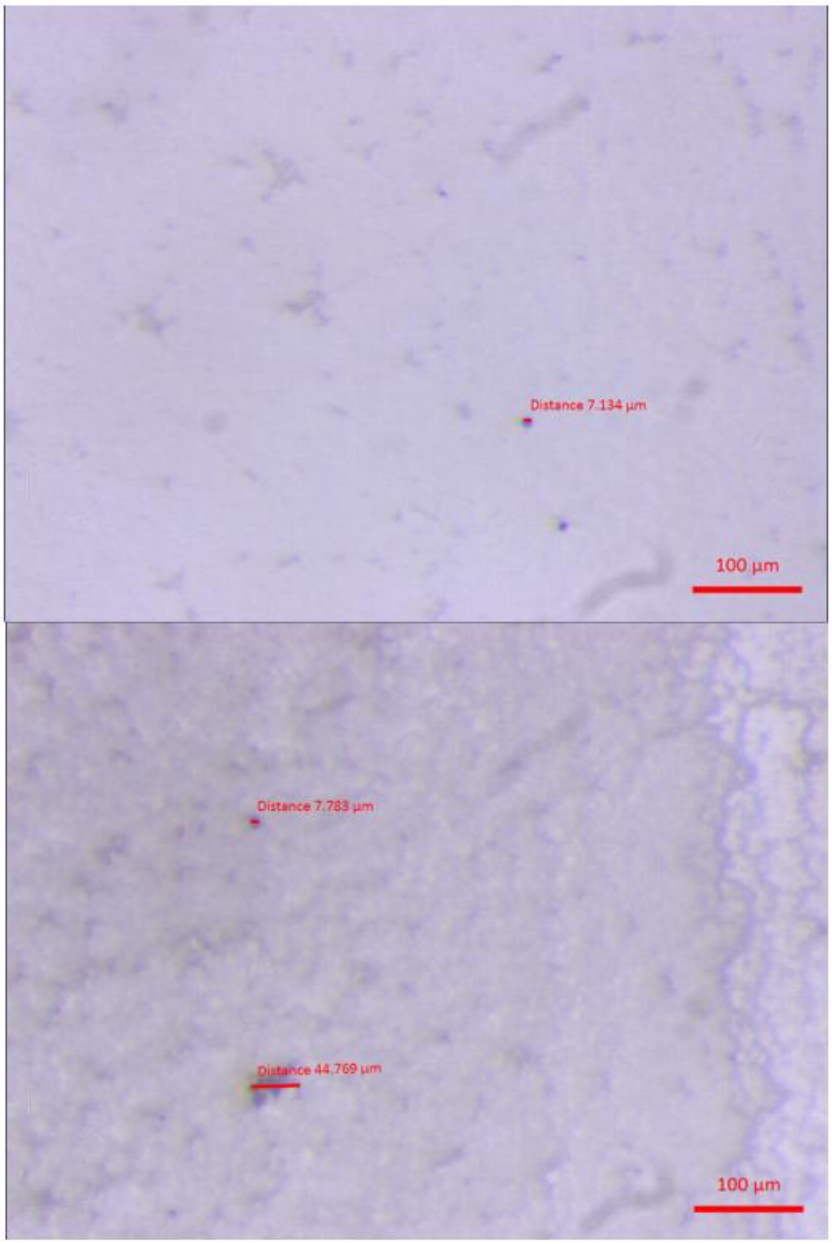


**Figure S1.** Optical microscopy of XGO showing most of the hydrogel monolith has been broken down into sub 10 micron particles, with a few agglomerations on the order of 10-50 microns.

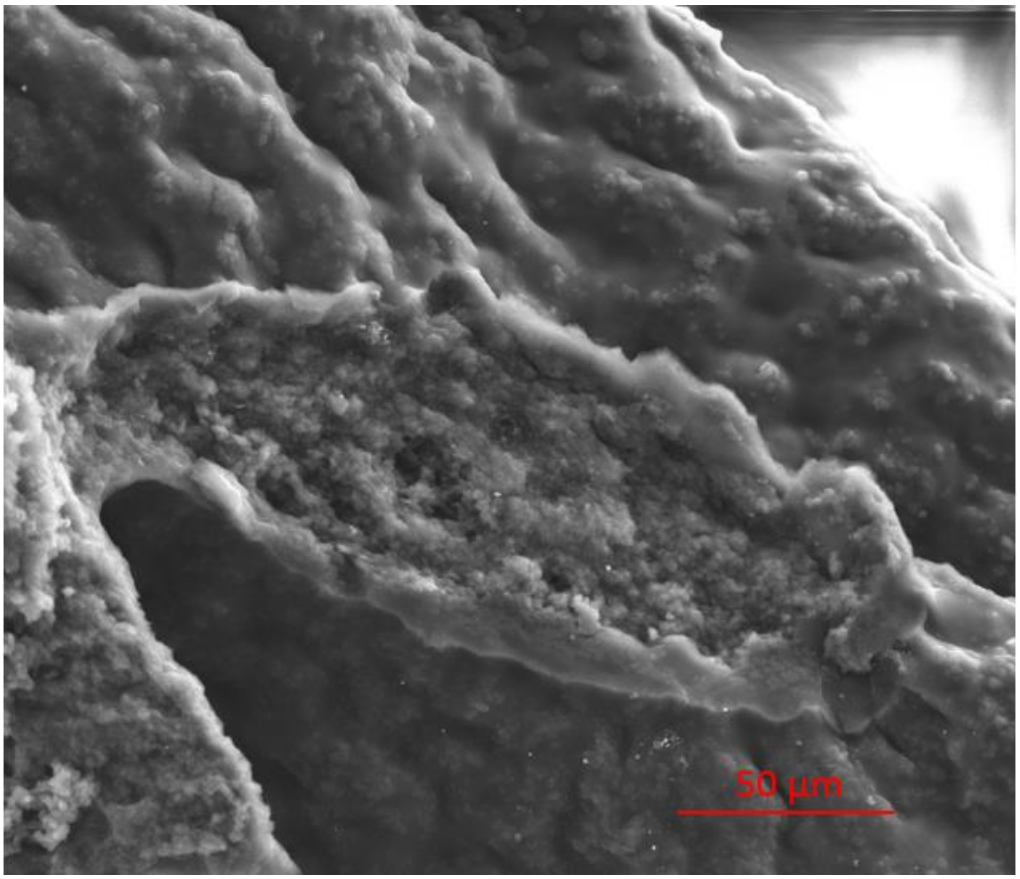


**Figure S2.** SEM of XGO with greater than 20wt% photopolymer showing the excessive amorphous carbon filling the pores of the 3DGs.

**Table 1**: Lattice shrinkage

| | Green Lattice | | | |
|---|---|---|---|---|
| | **Length (µm)** | **width (µm)** | **height (µm)** | **strut diameter (µm)** |
| | 969.57 | 971.71 | 491.53 | 89.88 |
| | 978.93 | 976.73 | 626.3 | 33.56 |
| | 906.26 | 906.18 | 559 | 94.43 |
| | 900.97 | 924.69 | 620.89 | 66.87 |
| | 895.6 | 915.05 | 524.68 | 83.77 |
| | 952.87 | 822.33 | 533.19 | 67.31 |
| **average** | 934.03 | 919.45 | 559.27 | 72.64 |
| | **Pyrolyzed Lattice** | | | |
| | **length (µm)** | **width (µm)** | **height (µm)** | **strut diameter (µm)** |
| | 407.19 | 426.52 | 340.22 | 30.26 |
| | 398.27 | 386.92 | | 33.64 |
| | 388.97 | 385.68 | | 22.25 |
| | 405.4 | 409.7 | | 33.65 |
| | 364.64 | | | 36.97 |
| **average** | 392.89 | 402.21 | 340.22 | 31.35 |
| **%change** | **-57.94%** | **-56.26%** | **-39.17%** | **-56.83%** |

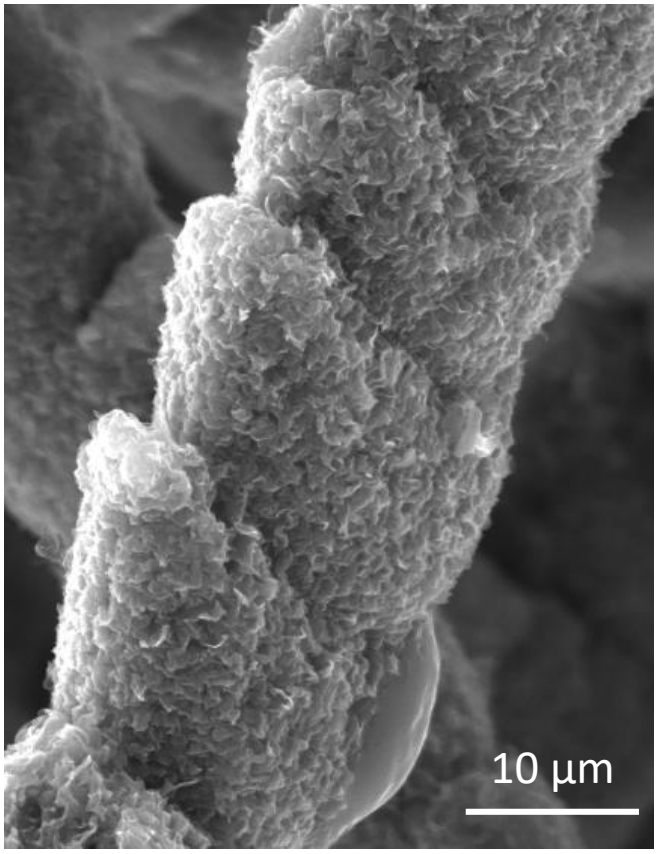


**Figure S3**. FGO MAG strut showing the small pore structure with lower surface area (47 $m^2/g$) compared to XGO with (130 $m^2/g$)

**Theoretical prediction of Young's modulus of the graphene lattices**

To describe the density dependency of the Young's modulus of the graphene lattices, we break down the graphene lattices into two length-scale hierarchies. On the microscale (first order structure), graphene can be modeled as a gyroid lattice.[3] On the macroscale (second order structure), the graphene lattices has a geometry called octet-truss lattice structure.[1,4] By extending the analysis presented by Lakes[5] for elasticity of hierarchical materials, we proposed a scaling model for the stiffness of the graphene lattices. Each scale level $n = [0,1,2 \dots N]$ within an $N$ order hierarchical structure can be represented by effective material properties dependent upon the order below it, where the $n = 0$ level is the base solid material with a Young's Modulus $E_s$.

The relative density of a hierarchical lattice with total number of hierarchy $n$ is given by:

$$\bar{\rho} = \prod_1^n \bar{\rho}_{i-(i-1)} \qquad (1)$$

where $\bar{\rho}_{i-(i-1)}$ is the relative density of material made up of the $i^{th}$ hierarchical level. For the graphene lattices shown in this work (N=2), the relative density can be written as,

$$\bar{\rho}_{2-0} = \bar{\rho}_{2-1}\bar{\rho}_{1-0} \qquad (2)$$

For the first order structure (gyroid), the effective Young's modulus is,

$$E_{1-0} = A(\bar{\rho}_{1-0})^{N_1} E_s \qquad (4)$$

where $A, \alpha$ are geometrical constants for gyroid lattices.

For second order structure (octet), the effective Young's modulus is,

$$E_{2-1} = B(\bar{\rho}_{2-1})^{N_2} E_{1-0} \qquad (5)$$

where $B, \beta$ are geometrical constants for octet-truss lattices.[1]

Here we have that $N_1 = 2.7$ (Gyroid),[3] $N_2 = 1.1$ (Octet)1

Substitute Eq. (4) into Eq. (5), the elastic modulus of the hierarchical graphene lattices becomes,

$$E_{2-0} = AB(\bar{\rho}_{2-1})^{N_2}(\bar{\rho}_{1-0})^{N_1} E_s \qquad (6)$$

By combining Eq. (2) and Eq. (6), the relationship between the relative density and elastic modulus of the hierarchical graphene lattices can be modified to,

$$\frac{E_{2-0}}{E_s} \sim (\bar{\rho}_{2-0})^{aN_1+bN_2}$$

where $a$ and $b$ quantify the contribution of the relative density change of the first and second order structure to the overall scaling, and satisfy the following relationship.

$$a = \frac{ln\bar{\rho}_{1-0}}{ln\bar{\rho}_{2-0}}.$$

$$b = \frac{ln\bar{\rho}_{2-1}}{ln\bar{\rho}_{2-0}},$$

$$(a + b = 1)$$

In our experiments, the variation range of $\bar{\rho}_{2-1}$ is much larger than $\bar{\rho}_{1-0}$, which means $b \gg a$. So the scaling of the effective elastic modulus of the graphene lattices is closer to $N_2$.

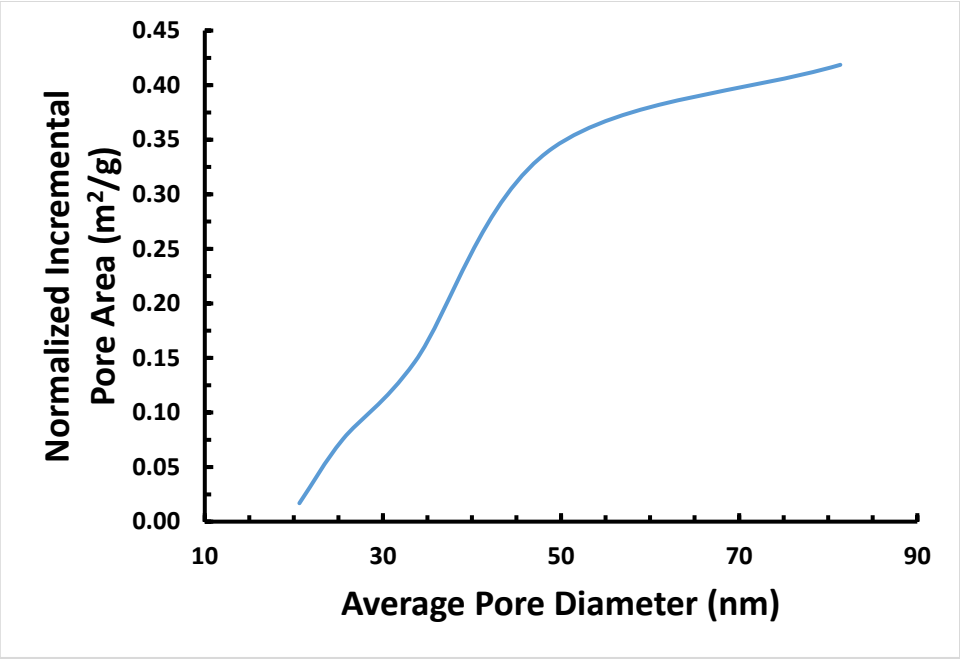


Figure S4: Pore size distribution of bulk MAG sample

**Table 2**: Conductivity of XGO materials

| Sample | Conductivity S/m | Density mg/cm$^3$ |
|---|---|---|
| **XGO Cube** | 38 | 469 |
| **10 mg/mL XGO** | 42 | |
| **7.5 mg/mL XGO** | 37 | |
| **5 mg/mL XGO** | 32 | |
| **XGO Lattice 1** | 64 | 92 |
| **XGO Lattice 2** | 63 | 100 |

The 10 mg/mL, 7.5 mg/mL and 5 mg/mL XGO samples are bulk cured resins with decreasing amounts (in mg/mL) of XGO. XGO Cube and XGO Lattice use 10 mg/mL concentration. Note, that XGO Lattice 1 and 2 were sputter coated with palladium to reduce contact resistance, which is the likely source of their increased conductivity.

**Table 3: MAGs Versus Literature Reported Graphene Properties**

| Name | Density ($mg/cm^3$) | Elastic Modulus (MPa) | Surface Area $m^2/g$ | Conductivity (S/m) | Maximum 3D Printed Resolution (μm) | Reference |
|---|---|---|---|---|---|---|
| XGO Stretch-Dominated | 92 | | 130 | 64 | 10 | This Work |
| | 100 | | | 63 | | |
| | 43.8 | 8.6 | | | | |
| | 49.5 | 8.4 | | | | |
| | 49.8 | 5.2 | | | | |
| | 90.8 | 37.9 | | | | |
| | 115.3 | 35.0 | | | | |
| | 170.1 | 43.3 | | | | |
| | 179.2 | 54.5 | | | | |
| | 200.6 | 78.6 | | | | |
| XGO Bend-Dominated | 47.6 | 0.6 | | | | |
| | 83.0 | 1.0 | | | | |
| Pristine Graphene | 2300 | 1020000 | 2600 | 8000 | | 1 |
| DIW GO Microlattices | 17 | 1.5 | 1066 | 87 | 250 | 2 |
| | 25 | 5 | 955 | 198 | | |
| | 55 | 25 | 704 | 278 | | |
| DIW GO-RF Lattices | 31 | 2 | | | | |
| | 60 | 4 | | | | |
| | 102 | 21 | | | | |
| 3D Freeze Printing Ref 1 | 0.5 | 0.1746 | | | 1500 | 3 |
| | 10 | | | 15.4 | 2000 | |
| 3D Freeze Printing Ref 2 | 17 | 0.84 | | | | 4 |
| | 6 | 0.13 | | 40 | | |
| Robocast GO | | | | | 100 | 5 |

| | | | | | | |
|---|---|---|---|---|---|---|
| PuSL Casting GLs | 8.33 | 1.05 | | | 2000 | 6 |
| Graphene Aerogels | 100 | 51 | 1314 | 100 | | 7 |
| Ultra-flyweight graphene | 0.16<br>0.75 | 4 | <br>272 | | | 8 |
| LIG Graphene Foam | 36<br>20 | 0.300<br>0.120 | 117.1<br>146.4 | 27<br>15 | 2000 | 9 |
| PI Graphene Foam | 7.6<br>12.2<br>18.0<br>24.5 | | | 1000<br>1144<br>1200<br>1335 | | 10 |

**Table 3 References**


| | |
|---|---|
| 1 | Bonaccorso, F. *et al.* Graphene, related two-dimensional crystals, and hybrid systems for energy conversion and storage. *Science* **347,** 1246501 (2015). |
| | Lee, C., Wei, X., Kysar, J. W. & Hone, J. Measurement of the Elastic Properties and Intrinsic Strength of Monolayer Graphene. *Science* **321,** 385–388 (2008). |
| | Qin, Z., Jung, G. S., Kang, M. J. & Buehler, M. J. The mechanics and design of a lightweight three-dimensional graphene assembly. *Science Advances* **3,** e1601536 (2017). |
| 2 | Zhu, C. *et al.* Highly compressible 3D periodic graphene aerogel microlattices. *Nature Communications* **6,** 6962 (2015). |
| 3 | Zhang, Q. *et al.* 3D Printing of Graphene Aerogels. *Small* **12,** 1702–1708 (2016). |
| 4 | Lin, Y. et al. Pristine Graphene Aerogels by Room-Temperature Freeze Gelation. Adv. Mater. 28, 7993–8000 (2016). |
| 5 | García-Tuñon, E. *et al.* Printing in Three Dimensions with Graphene. *Adv. Mater.* **27,** 1688–1693 (2015). |
| 6 | Zhang, Q., Zhang, F., Xu, X., Zhou, C. & Lin, D. Three-Dimensional Printing Hollow Polymer Template-Mediated Graphene Lattices with Tailorable Architectures and Multifunctional Properties. *ACS Nano* (2018). doi:10.1021/acsnano.7b06095 |

| | |
|---|---|
| 7 | Worsley, M. A. *et al.* Mechanically robust 3D graphene macroassembly with high surface area. *Chem. Commun.* **48,** 8428–8430 (2012). |
| 8 | Sun, H., Xu, Z. & Gao, C. Multifunctional, Ultra-Flyweight, Synergistically Assembled Carbon Aerogels. *Adv. Mater.* **25,** 2554–2560 (2013). |
| 9 | Luong, D. X. *et al.* Laminated Object Manufacturing of 3D-Printed Laser-Induced Graphene Foams. *Advanced Materials* **0,** 1707416 |
| 10 | J. Liu, Y. Liu, H.-B. Zhang, Y. Dai, Z. Liu and Z.-Z. Yu, *Carbon*, 2018, **132**, 95–103. |

**Supplementary Information References:**


1. Zheng, X. *et al.* Ultralight, ultrastiff mechanical metamaterials. *Science* **344,** 1373–1377 (2014).

2. Cui, H., Hensleigh, R., Chen, H. & Zheng, X. Additive Manufacturing and size-dependent mechanical properties of three-dimensional microarchitected, high-temperature ceramic metamaterials. *J. Mater. Res.* **33,** 360–371 (2018).

3. Qin, Z., Jung, G. S., Kang, M. J. & Buehler, M. J. The mechanics and design of a lightweight three-dimensional graphene assembly. *Sci. Adv.* **3,** e1601536 (2017).

4. Zheng, X. *et al.* Multiscale metallic metamaterials. *Nat. Mater.* **15,** 1100 (2016).

5. Lakes, R. Materials with structural hierarchy. *Nature* (1993). doi:10.1038/361511a0